

# Dual polarization nonlinear Fourier transform-based optical communication system

S. GAIARIN<sup>1,\*</sup>, A. M. PEREGO<sup>2,\*</sup>, E. P. DA SILVA<sup>1</sup>, F. DA ROS<sup>1</sup>, AND D. ZIBAR<sup>1</sup>

<sup>1</sup>DTU Fotonik, Technical University of Denmark, Lyngby, 2800 Denmark

<sup>2</sup>Aston Institute of Photonic Technologies, Aston University, Aston Express Way, Birmingham, B4 7ET UK

\*Corresponding authors: [simga@fotonik.dtu.dk](mailto:simga@fotonik.dtu.dk), [peregoa@aston.ac.uk](mailto:peregoa@aston.ac.uk)

Compiled March 6, 2018

---

New services and applications are causing an exponential increase in internet traffic. In a few years, current fiber optic communication system infrastructure will not be able to meet this demand because fiber nonlinearity dramatically limits the information transmission rate. Eigenvalue communication could potentially overcome these limitations. It relies on a mathematical technique called "nonlinear Fourier transform (NFT)" to exploit the "hidden" linearity of the nonlinear Schrödinger equation as the master model for signal propagation in an optical fiber. We present here the theoretical tools describing the NFT for the Manakov system and report on experimental transmission results for dual polarization in fiber optic eigenvalue communications. A transmission of up to 373.5 km with bit error rate less than the hard-decision forward error correction threshold has been achieved. Our results demonstrate that dual-polarization NFT can work in practice and enable an increased spectral efficiency in NFT-based communication systems, which are currently based on single polarization channels.

*OCIS codes:*

---

## 1. INTRODUCTION

Fiber optics telecommunication is the currently established backbone infrastructure for most of the information flow across the world [1]. However, the demand for an always increasing transmission rate, which for the existing channels is necessarily associated with an increment of the launched signal power to minimize the optical signal-to-noise ratio (OSNR) degradation, has been predicted to be asymptotically limited by the distortion induced by the optical fiber nonlinearity [2, 3]. It is a well-known fact that light propagation in fiber optics is governed by the nonlinear Schrödinger equation (NLSE) [4] where the nonlinearity arises due to the Kerr effect. Nonlinearity is a problem for transmitting information with the currently used modulation formats in fiber optics communications. Indeed, as the power is increased, the signal is more distorted by the nonlinear cross-talk, thus limiting the capability of the receiver in recovering the transmitted information. It is therefore necessary to mitigate the nonlinear effects to compensate for the distortions and to provide novel approaches for the communication over the nonlinear fiber-optic channel. Two main paths have been followed up to now to counteract this problem: the first approach

consists in mitigating the nonlinear effects through a wealth of techniques such as for instance optical phase-conjugation [5] or digital back-propagation [6]; the second path, more ambitiously, aims at encoding information into the eigenmodes of the nonlinear channel, whose evolution is linear upon spatial propagation. This second approach, originally called *Eigenvalue communication*, has been proposed by Hasegawa and Nyu [7] and it is now, with various modifications, growing as a new paradigm in optical communications [8].

This method exploits the exact integrability of the NLSE through the inverse scattering transform (IST) [9] as the master evolution equation of the electric field propagating in single mode fiber (SMF). Integrability of the NLSE was demonstrated by Zakharov and Shabat back in 1972 [10], who found an associated spectral problem, related to a set of ordinary linear differential equations. Following this approach, it is possible to identify the eigenvalues, that can be considered the analogous of the frequencies in the classical Fourier transform; and the so called scattering coefficients: complex amplitudes associated to the eigenvalues. The application of the IST to fiber optics communications allows the use of various and flexible modulation

formats [8]. Due to integrability, in the lossless and noiseless limit, nonlinearity is not a detrimental factor anymore, but on the contrary, it is a constitutive element of the transmission system itself. The parallelism between the linear Fourier transform method used to solve linear initial value problems and the IST used to solve nonlinear ones [9], has driven some authors to rename the IST as nonlinear Fourier transform (NFT) [11], which is the name currently used in the engineering communities (see [8] for a recent review including historical details). The nonlinear Fourier spectrum of a signal consists of a set of eigenvalues and the respective associated scattering coefficients. The eigenvalues belong either to a so-called *discrete spectrum* or to a *continuous spectrum*; the first describes the solitonic components of the signal, while the second is associated with dispersive waves and reduces to the classical Fourier spectrum in the limit of low power.

Communications channels based on both discrete or/and continuous spectrum modulations have been extensively studied and experimentally demonstrated up to now for the scalar (single polarization) NLSE (see e.g. [12–16] to cite just a few).

A series of key challenges that need to be met in order to bring NFT-based communication to exit the labs and operate in real-world infrastructures, has been described recently [8]. One of those challenges consists indeed of endowing the *Eigenvalue communication* approach with polarization division multiplexing, which allows information to be encoded on both orthogonal polarization components supported by SMFs. The description of the light propagation, accounting for its polarization dynamics can, under specific conditions that apply to modern communications fiber link, be described by the Manakov equations [17]. In a milestone paper of nonlinear science, Manakov showed that those equations can be solved analytically by the IST [18]. Detailed investigations of the solutions of the Manakov equations especially concerning soliton and multisoliton dynamics in presence of noise and polarization mode dispersion (PMD) in optical communications, as well as their connection with optical rogue waves formation, are present in the literature [19–25].

To the best of our knowledge the NFT dual polarization problem has never been tackled at the level to demonstrate a working communication system and only very preliminary theoretical works are present in the literature on this topic [26, 27].

In this article, we present the mathematical framework underlying the dual polarization NFT and we show an extension of our recent results on the first experimental demonstration of a dual polarization nonlinear frequency division multiplexing (DP-NFDM) fiber optics communication system [28]. We have transmitted up to 373.5 km at the hard-decision forward error correction (HD-FEC) bit error rate (BER) threshold of  $3.8 \times 10^{-3}$ , with information encoded in the quadrature phase shift keying (QPSK) modulated scattering coefficients associated with two eigenvalues belonging to the Manakov system discrete spectrum, for both orthogonal polarization components supported by a SMF.

The structure of the paper is the following: in section 2 we will first define the NFT for the dual polarization case and describe the mathematical tools -the Darboux transformation (DT)- needed to generate the waveforms associated with a desired nonlinear spectrum for both field polarizations. In section 3 we will discuss the details of a DP-NFDM system. Finally, in section 4 we present a detailed account of the experimental transmission results, followed by a discussion of the results and conclusions in section 5.

## 2. MATHEMATICAL FRAMEWORK

### A. Channel model

The evolution of the slowly varying complex-valued envelopes of the electric field propagating in a SMF exhibiting random birefringence and whose dispersion and nonlinear lengths are much larger than the birefringence correlation length, is described by the averaged Manakov equations [17, 29]

$$\begin{cases} \frac{\partial E_1}{\partial \ell} = -i\frac{\beta_2}{2}\frac{\partial^2 E_1}{\partial \tau^2} + i\frac{8\gamma}{9}\left(|E_1|^2 + |E_2|^2\right)E_1 \\ \frac{\partial E_2}{\partial \ell} = -i\frac{\beta_2}{2}\frac{\partial^2 E_2}{\partial \tau^2} + i\frac{8\gamma}{9}\left(|E_1|^2 + |E_2|^2\right)E_2 \end{cases} \quad (1)$$

where  $\tau$  and  $\ell$  represent the time and space coordinates,  $E_j$ ,  $j = 1, 2$  are the amplitudes of the two electric field polarizations,  $\beta_2$  is the dispersion coefficient and  $\gamma$  is the nonlinearity coefficient.

In order to remove any dependency from a specific channel, it is common to work with the normalized version of Eq. (1). The normalized Manakov system (MS) [18, 30, 31] is obtained by performing the change of variable

$$q_j = \frac{E_j}{\sqrt{P}}, \quad t = \frac{\tau}{T_0}, \quad z = -\frac{\ell}{\mathcal{L}} \quad (2)$$

with  $P = |\beta_2|/(\frac{8}{9}\gamma T_0^2)$ ,  $\mathcal{L} = 2T_0^2/|\beta_2|$  and  $T_0$  is a free normalization parameter, leading to

$$\begin{cases} i\frac{\partial q_1}{\partial z} = \frac{\partial^2 q_1}{\partial t^2} + 2\left(|q_1|^2 + |q_2|^2\right)q_1 \\ i\frac{\partial q_2}{\partial z} = \frac{\partial^2 q_2}{\partial t^2} + 2\left(|q_1|^2 + |q_2|^2\right)q_2 \end{cases} \quad (3)$$

where  $z$  and  $t$  represent the normalized space and time variables respectively. In this study we have considered the anomalous dispersion regime ( $\beta_2 < 0$ ), since it is the one that supports solitons and corresponds to the regime of currently deployed SMFs.

In realistic systems the field amplitude is attenuated upon spatial propagation at a rate  $\alpha/2$ , where  $\alpha$  is the attenuation coefficient of the fiber. This breaks the integrability of Eq. (1). However it is possible to suitably redefine the fields  $E_{1,2} \rightarrow E_{1,2}e^{-(\alpha/2)\ell}$  in such a way that they obey a lossless equation with an effective nonlinearity coefficient

$$\gamma_{eff} = \gamma\left(1 - e^{-\alpha L}\right)/(\alpha L) \quad (4)$$

where  $L$  is the length of one optical fiber span. The evolution equation with the modified nonlinear term can be considered the leading approximation of the lossy system when we account for the periodic signal boosts due to the erbium-doped fiber amplifiers (EDFAs). This is the so-called lossless path-averaged (LPA) model [32–34], which is in general valid when the amplifiers spacing is smaller than the soliton period, and it has been used across all the present study.

### B. Direct NFT

In order to compute the NFT of a signal  $q_{1,2}(t)$  it is first necessary to associate to the MS Eq. (3) a so-called spectral problem. This is known for the case of the NLSE as the Zakharov-Shabat spectral problem (ZSP), while for the Manakov equations we can call it the Manakov-Zakharov-Shabat spectral problem (MZSP). The

MZSP is defined by the following system of linear ordinary differential equations

$$\frac{\partial v}{\partial t} = (\lambda \mathbf{A} + \mathbf{B}) v \quad (5)$$

being

$$\mathbf{A} = \begin{pmatrix} -i & 0 & 0 \\ 0 & i & 0 \\ 0 & 0 & i \end{pmatrix} \quad \mathbf{B} = \begin{pmatrix} 0 & q_1 & q_2 \\ -q_1^* & 0 & 0 \\ -q_2^* & 0 & 0 \end{pmatrix}$$

where  $v$  is a solution and  $\lambda$  is a spectral parameter.

Assuming the vanishing boundary conditions for the signal, i.e.,  $|q_{1,2}(t)| \rightarrow 0$  for  $t \rightarrow |\infty|$ , it is possible to find a set of canonical solutions to Eq. (5) called Jost solutions defined as [30]:

$$\phi^N(t, \lambda) \rightarrow \begin{pmatrix} 1 \\ 0 \\ 0 \end{pmatrix} e^{-i\lambda t}; \quad \bar{\phi}^N(t, \lambda) \rightarrow \begin{pmatrix} 0 & 0 \\ 1 & 0 \\ 0 & 1 \end{pmatrix} e^{i\lambda t} \quad t \rightarrow -\infty \quad (6a)$$

$$\phi^P(t, \lambda) \rightarrow \begin{pmatrix} 0 & 0 \\ 1 & 0 \\ 0 & 1 \end{pmatrix} e^{i\lambda t}; \quad \bar{\phi}^P(t, \lambda) \rightarrow \begin{pmatrix} 1 \\ 0 \\ 0 \end{pmatrix} e^{-i\lambda t} \quad t \rightarrow +\infty. \quad (6b)$$

$\{\phi^P(t, \lambda), \bar{\phi}^P(t, \lambda)\}$  and  $\{\phi^N(t, \lambda), \bar{\phi}^N(t, \lambda)\}$  are two bases for the eigenspace associate to  $\lambda$ . One can write  $\phi^N(t, \lambda)$  and  $\bar{\phi}^N(t, \lambda)$  as a linear combination of the basis vectors  $\{\phi^P(t, \lambda), \bar{\phi}^P(t, \lambda)\}$  as

$$\phi^N(t, \lambda) = \phi^P(t, \lambda)b(\lambda) + \bar{\phi}^P(t, \lambda)a(\lambda) \quad (7a)$$

$$\bar{\phi}^N(t, \lambda) = \phi^P(t, \lambda)\bar{a}(\lambda) + \bar{\phi}^P(t, \lambda)\bar{b}(\lambda) \quad (7b)$$

with coefficients  $a(\lambda)$ ,  $b(\lambda)$ ,  $\bar{a}(\lambda)$  and  $\bar{b}(\lambda)$ , where  $a(\lambda)$  is a scalar,  $\bar{a}(\lambda)$  is a  $2 \times 2$  matrix,  $b(\lambda)$  is a two entries column vector and  $\bar{b}(\lambda)$  is a two entries row vector. These coefficients are called scattering coefficients. From the knowledge of the scattering coefficients, it is possible to reconstruct the signal  $q_{1,2}(t)$  uniquely.

Analogously to the case of the NLSE [11] we can define the NFT continuous and discrete spectral amplitudes for the MS as:

$$Q_c(\lambda) = b(\lambda)a(\lambda)^{-1} \quad \lambda \in \mathbb{R} \quad (8a)$$

$$Q_{d,i}(\lambda_i) = b(\lambda_i)a'(\lambda_i)^{-1} \quad \lambda_{1,\dots,n} \in \mathbb{C} \setminus \mathbb{R} \quad (8b)$$

and  $a'(\lambda_i) = \frac{da(\lambda)}{d\lambda}|_{\lambda=\lambda_i} \forall \lambda_{1,\dots,n} \in \mathbb{C} \setminus \mathbb{R}$  such that  $a(\lambda_i) = 0$ . Although these spectral amplitudes are commonly used, it is more convenient to work directly with the scattering coefficients  $a(\lambda)$  and  $b(\lambda)$  [35]; hence, when throughout the whole manuscript we will refer to the nonlinear spectrum, we will implicitly mean the eigenvalues and the associated scattering coefficients. The scattering coefficients are time independent and their spatial evolution is given by [30]:

$$a(\lambda, z) = a(\lambda, 0) \quad \bar{a}(\lambda, z) = \bar{a}(\lambda, 0) \quad (9a)$$

$$b(\lambda, z) = b(\lambda, 0)e^{-4i\lambda^2 z} \quad \bar{b}(\lambda, z) = \bar{b}(\lambda, 0)e^{4i\lambda^2 z}. \quad (9b)$$

In order to not overburden the notation we will drop the explicit space dependence as we did in the beginning of this section. The fact that the scattering coefficients are time invariant, allows computing them at an arbitrary instant of time. For example,

using Eq. (7a) and the boundary Jost solutions, they can be computed at  $t = +\infty$ . At this instant  $\phi^P(t, \lambda)$  is known. Moreover, it is possible to propagate  $\phi^N(t, \lambda)$  from  $t = -\infty$ , where it is known, to  $t = +\infty$  by integrating Eq. (7a). Given the particular structure of the Jost solutions it results that the scattering coefficients are given by:

$$a(\lambda) = \lim_{t \rightarrow +\infty} [\phi_1^N(t, \lambda)\bar{\phi}_1^P(t, \lambda)^{-1}] \quad (10a)$$

$$b_1(\lambda) = \lim_{t \rightarrow +\infty} [\phi_2^N(t, \lambda)\phi_{2,1}^P(t, \lambda)^{-1}] \quad (10b)$$

$$b_2(\lambda) = \lim_{t \rightarrow +\infty} [\phi_3^N(t, \lambda)\phi_{3,2}^P(t, \lambda)^{-1}] \quad (10c)$$

and using Eq. (6) and Eq. (7a) gives

$$a(\lambda) = \lim_{t \rightarrow +\infty} [\phi_1^N(t, \lambda)e^{i\lambda t}] \quad (11a)$$

$$b(\lambda) = \begin{pmatrix} b_1(\lambda) \\ b_2(\lambda) \end{pmatrix} = \lim_{t \rightarrow +\infty} \left[ \begin{pmatrix} \phi_2^N(t, \lambda) \\ \phi_3^N(t, \lambda) \end{pmatrix} e^{-i\lambda t} \right]. \quad (11b)$$

It should be noted that, compared to the NLSE case, there is an additional scattering coefficient  $b_2(\lambda)$  that can be used to encode information, potentially doubling the system transmission rate.

### C. Inverse NFT

The inverse nonlinear Fourier transform (INFT) is the mathematical procedure that allows constructing a time domain waveform starting from a given nonlinear spectrum. In our work, we have performed the INFT at the transmitter by using an algorithm based on the DT [36]. The DT is a natural candidate to build time domain signals, especially when the information is encoded only in the discrete nonlinear spectrum. The method consists in adding iteratively discrete eigenvalues to the nonlinear spectrum while simultaneously updating the signal in time domain. The INFT based on the DT for eigenvalue communications was proposed in [37]. In our work we have used the DT for the MS derived by Wright [38]. We summarize here how the DT for the MS works.

Let  $v$  be a column vector solution of the MZSP spectral problem Eq. (5) associated with the MS for the signal  $q(t)$  and the eigenvalue  $\lambda$ , then according to [38] a new solution of Eq. (5),  $\hat{v}$ , is given by the following equation:

$$\hat{v} = (\lambda \mathbf{I}_3 - \mathbf{G}_0) v \quad (12)$$

where  $\mathbf{I}_3$  is the  $3 \times 3$  identity matrix,  $\mathbf{G}_0 = \Theta \mathbf{M}_0 \Theta^{-1}$  with

$$\Theta = \begin{pmatrix} \bar{v}_1 & \bar{v}_2^* & \bar{v}_3^* \\ \bar{v}_2 & -\bar{v}_1^* & 0 \\ \bar{v}_3 & 0 & -\bar{v}_1^* \end{pmatrix} \quad (13)$$

where the matrix  $\mathbf{M}_0 = \text{diag}(\lambda_0, \lambda_0^*, \lambda_0^*)$  and  $\bar{v} = (\bar{v}_1, \bar{v}_2, \bar{v}_3)^T$  is a solution of Eq. (5) for the seed signal  $q_j$ ,  $j = 1, 2$  and a fixed value of  $\lambda = \lambda_0$ . The DT gives the new signal waveforms in time domain for both polarizations  $\hat{q}_j$ ,  $j = 1, 2$  as a function of the old signals  $q_j$ , of the auxiliary solution  $\bar{v}$  and of the new eigenvalue  $\lambda_0$  we want to add to the nonlinear spectrum:

$$\hat{q}_j = q_j + 2i(\lambda_0^* - \lambda_0) \frac{u_j^*}{1 + \sum_{s=1}^2 |u_s|^2} \quad (j = 1, 2) \quad (14)$$

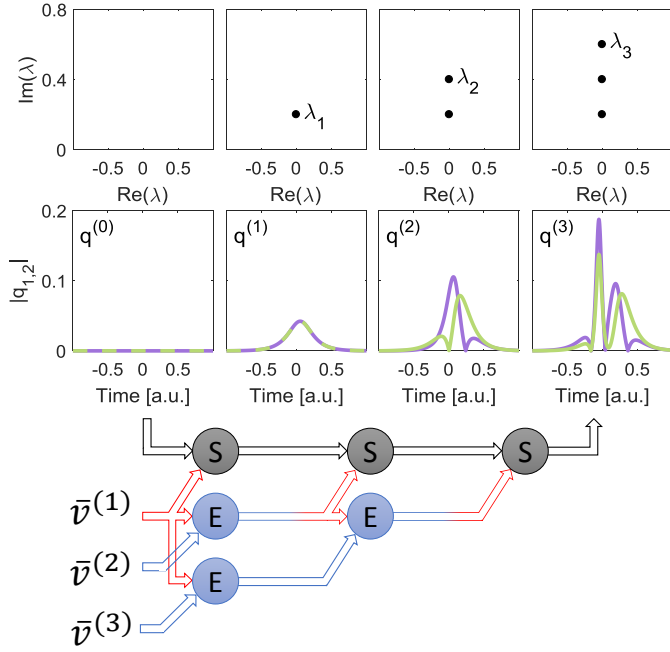


**Fig. 1.** Schematic of the DT. The S-node is the signal update operation corresponding to Eq. (14) and the E-node is the eigenvector update operation corresponding to Eq. (12). At the step  $i = 1, 2, 3$  the auxiliary solution  $\bar{v}^{(i)}$  for  $\lambda = \lambda_i$  (red arrow) modifies the signal  $q_j^{(i-1)}$  and all the other auxiliary solutions (blue arrows). The seed null signal  $q_j^{(0)}$ ,  $j = 1, 2$  entering the first S-node is transformed after each step in such a way that its discrete spectrum has a new eigenvalue added as shown in the four insets in upper part of the figure.

where  $u_j = \bar{v}_{j+1}/\bar{v}_1$ .

Starting from the "vacuum" solution  $q_j(t) = 0$ ,  $j = 1, 2$ , the procedure sketched in Fig. 1 can be repeated iteratively to generate the dual polarization time domain signal associated with a nonlinear spectrum containing an arbitrary large number of discrete eigenvalues.

The generic auxiliary solution  $\bar{v}^{(k)}$  that satisfies the MZSP for the eigenvalue  $\lambda_k$  reads:  $\bar{v}^{(k)} = (A^{(k)}e^{-i\lambda_k t}, B^{(k)}e^{i\lambda_k t}, C^{(k)}e^{i\lambda_k t})^T$  (being  $\{A^{(k)}, B^{(k)}, C^{(k)}\}$  some initialization constants). Hence after adding  $i$  eigenvalues the auxiliary solutions are modified according to the following chain of matrix multiplications

$$\begin{pmatrix} \hat{\bar{v}}_1^{(k)} \\ \hat{\bar{v}}_2^{(k)} \\ \hat{\bar{v}}_3^{(k)} \end{pmatrix} = (\lambda_k \mathbf{I}_3 - \mathbf{G}_{0i-1}) \dots (\lambda_k \mathbf{I}_3 - \mathbf{G}_{01}) \begin{pmatrix} A^{(k)} e^{-i\lambda_k t} \\ B^{(k)} e^{i\lambda_k t} \\ C^{(k)} e^{i\lambda_k t} \end{pmatrix} \quad (15)$$

where the  $\mathbf{G}_{0i}$  matrices are evaluated as functions of the  $i$ -th auxiliary solution  $\bar{v}^{(i)}$  evaluated after  $i - 1$  Darboux transformations, see also the scheme depicted in Fig. 1. The initialization constants  $\{A^{(k)}, B^{(k)}, C^{(k)}\}$  have been set respectively equal to  $\{1, -b_1(\lambda_k), -b_2(\lambda_k)\}$ , in order to obtain the correct spectrum after performing NFT and INFT in sequence as in the scalar case [39].  $b_1(\lambda_k)$  and  $b_2(\lambda_k)$  are the scattering coefficients that we want to associate to the eigenvalue  $\lambda_k$  for the two polarization components respectively.

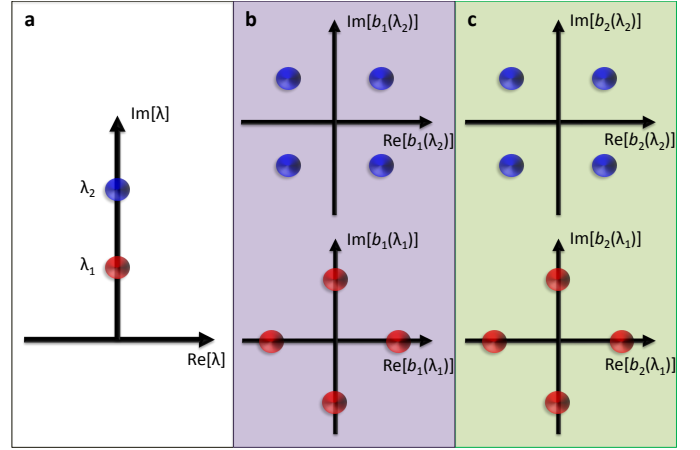


**Fig. 2.** Ideal normalized constellations are illustrated schematically: in (a) the discrete eigenvalues  $\lambda_1 = i0.3$  and  $\lambda_2 = i0.6$  are depicted. The scattering coefficients  $b_{1,2}(\lambda_i)$ ,  $i = 1, 2$ , associated with the two orthogonal polarization components of the signal, are shown in (b) and (c) respectively. Polarization 1 and Polarization 2 on a violet and green background respectively. The scattering coefficients associated with  $\lambda_1$  are chosen from a QPSK constellation of radius 5 and rotated by  $\pi/4$  while those associated with  $\lambda_2$  from a QPSK constellation and radius 0.14.

### 3. DP-NFDM SYSTEM

In this section, the basic structure of a DP-NFDM system using the discrete spectrum will be described. The digital signal processing (DSP) chain will be introduced first and then the experimental setup.

#### A. Transmitter and receiver digital signal processing

At the transmitter the data bits are mapped to the scattering coefficients pairs  $\{b_1(\lambda_i), b_2(\lambda_i)\}$  for  $i = 1, 2$  where the pair of eigenvalues  $\{\lambda_1 = i0.3, \lambda_2 = i0.6\}$  is used for each symbol. We will refer to these set of coefficients and equivalently to the associated time domain waveform as a DP-NFDM symbol. The scattering coefficients associated with the first eigenvalue can assume values drawn from a QPSK constellation of radius 5 and rotated by  $\pi/4$  while those associated with the second eigenvalue are drawn from a QPSK constellation of radius 0.14 as shown in Fig. 2. This particular structure of the constellations was chosen to reduce the peak-to-average power ratio (PAPR) of the signal at the transmitter, in order to limit the performance losses due to the limited resolution of the digital-to-analog converter (DAC) and due to the nonlinear characteristic of Mach-Zehnder modulators (MZMs) and electrical amplifiers (See Supplementary Material for a detailed explanation). The waveform associated to each DP-NFDM symbol is generated using the DT described in the previous section followed by the denormalization as in Eq. (2) with normalization parameter  $T_0 = 47$  ps. This choice of  $T_0$  allows fitting the waveform in a time window of 1 ns (1 Gbd) with enough time guard band among successive DP-NFDM symbols to satisfy the vanishing boundary conditions required to correctly compute the NFT. The power  $P_{tx}$  of the digital signal thus obtained will later be used to set the power of the corresponding transmitted optical signal.

The channel is assumed to be a link of standard SMF with EDFA lumped amplification as in the experiment. In order to

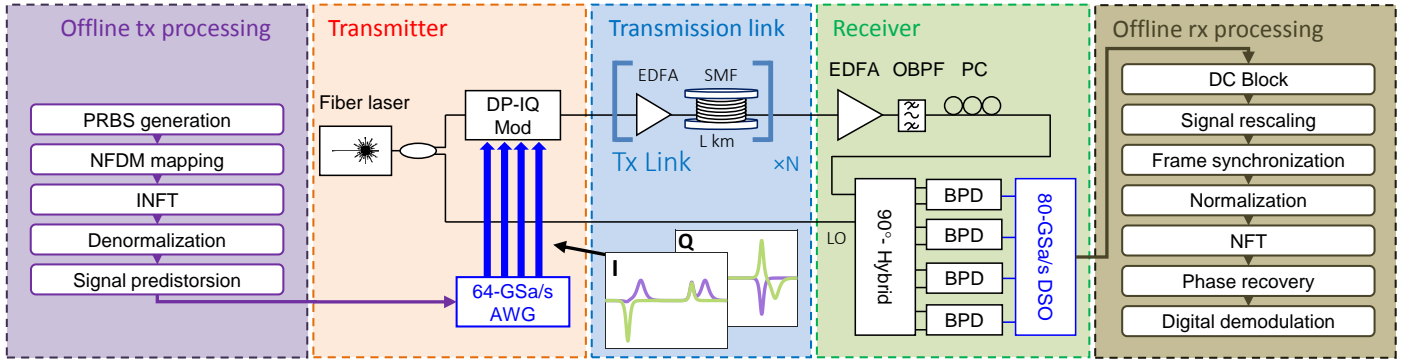


**Fig. 3.** Experimental setup with transmitter and receiver DSP chain. Abbreviations not defined in the main text: balanced photodetector (BPD), direct current (DC).

take into account the presence of the losses, the LPA approximation is used in the normalization and denormalization steps of the waveform before computing the NFT and after computing the INFT respectively.

At the receiver, the digital signal output by the digital storage oscilloscope (DSO) is first rescaled so that its power is  $P_{tx}$  (the power of the transmitted optical signal). Then an ideal rectangular filter with bandwidth equal to the 99% power bandwidth of the signal is used to filter the out of band noise. At this point, cross-correlation-based frame synchronization using training sequences is performed in order to optimally align the DP-NFDM symbol to the processing window. For each DP-NFDM symbol, first the eigenvalues are located using the Newton-Raphson search method employing the one-directional trapezoidal method and then the coefficients  $b_{1,2}(\lambda_i)$  are computed on the found eigenvalues using the forward-backward trapezoidal method (see Supplementary Material for more details). The homodyne configuration of the receiver allows not having a frequency offset between the transmitter laser and the coherent receiver local oscillator (LO), but given the non-zero combined linewidth of the two lasers ( $\sim 1$  kHz) their coherence length is limited to about 90 km. This implies that the received constellations are affected by phase noise when the transmission distance exceeds the coherence length of the laser, causing errors

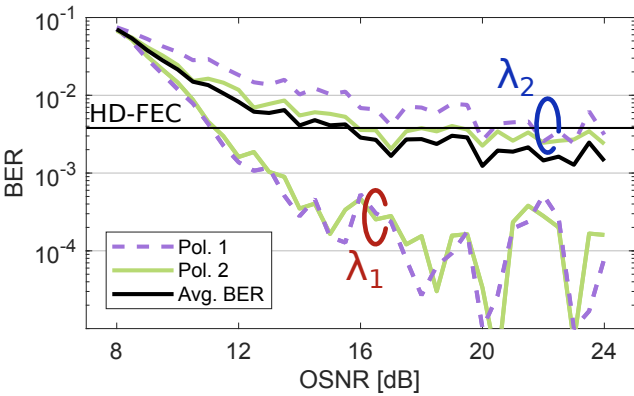


**Fig. 4.** System performance in terms of BER as a function of the OSNR in a back-to-back configuration. The BER of the individual constellations are shown by the violet (Polarization 1) and green (Polarization 2) curves and are grouped per eigenvalue ( $\lambda_1 = i0.3$ ,  $\lambda_2 = i0.6$ ). The black curve represents the average BER over the 4 constellations.

in the detection of the symbols. The phase noise is removed by applying the blind phase search algorithm [40] in the NFT domain to each constellation individually. Finally, the scattering coefficients are rotated back to remove the phase factor acquired during the transmission (Eq. (9b)) and the decision on the symbols is taken using a minimum Euclidean distance decisor over the scattering coefficients.

## B. Experimental setup

The experimental setup and the block diagrams of the DSP are depicted in Fig. 3. At the transmitter a fiber laser (FL) with sub-kHz linewidth is modulated using an integrated dual polarization I/Q modulator driven by an arbitrary waveform generator (AWG) with 20 GHz analog bandwidth and 64 GSa/s. Before uploading it to the AWG, the signal generated by the INFT is pre-distorted using the ideal inverse transfer function of the MZM ( $\text{asin}(\cdot)$ ). This pre-distortion is required in order to have a good trade-off between signal-to-noise ratio (SNR) at the output of the MZM and signal distortions caused by its nonlinear transfer function. Nonetheless, given the still high PAPR of the optimized waveform considered (see Supplementary Material), this pre-distortion is not optimal and advanced methods can be employed to improve further the quality of the transmitted signal [41]. The channel is a fiber link composed of up to 9 spans of SMF fiber with dispersion  $D = 17.5$  ps/nm·km, nonlinear coefficient  $\gamma = 1.25$  W<sup>-1</sup>km<sup>-1</sup>, attenuation  $\alpha = 0.195$  dB/km and PMD coefficient  $< 0.1$  ps km<sup>-1/2</sup>. Two different span lengths of  $L = 41.5$  and  $L = 83$  km were employed. Considering these channel parameters, the complex baseband signal generated by the INFT with LPA and denormalized has the following properties: 99% of its power contained within a bandwidth  $W$  of 12.7 GHz, a PAPR of 9.49 dB and an average power  $P_{tx}$  of 5.30 dBm and 7.70 dBm for the span lengths  $L$  of 41.5 and 83 km, respectively. Given these channel and signal parameters we have that the soliton period, defined as  $(\pi/2)L_d$ , with  $L_d = (W|\beta_2|)^{-1}$  the dispersion length [8, 42], is 436 km. Being this much larger than the typical birefringence correlation length, which is on a scale of few tens of meters [29], guarantees the applicability of the Manakov averaged model.

In order to properly match the transmitted signal to the channel, the gain of the EDFA at the transmitter is tuned in such a way to set the power of the optical signal to  $P_{tx}$ . The optical signal is then transmitted through the channel.

At the receiver, the signal is first sent through a 0.9 nm optical band pass filter (OBPF) and then a polarization controller (PC) was used to manually align the polarization of the signal to

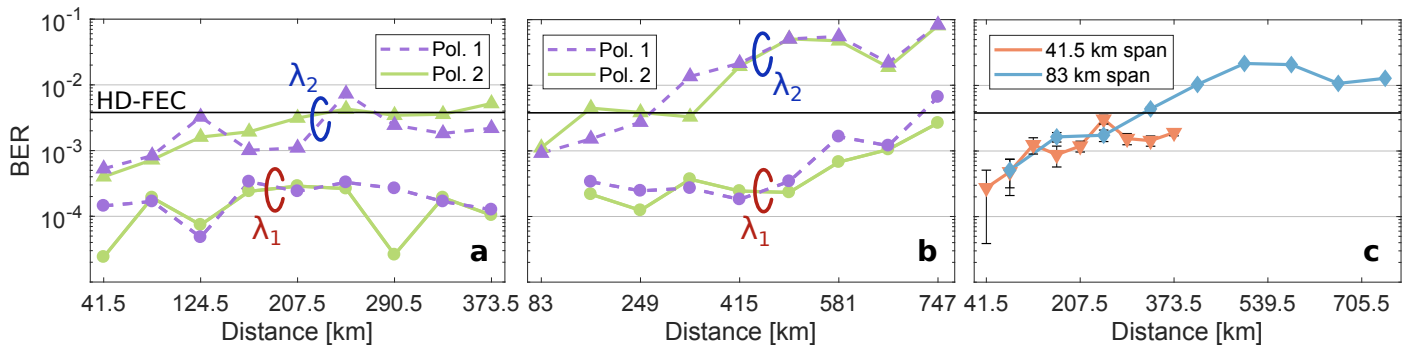


**Fig. 5.** System performance in terms of BER as a function of the transmission distance for the 4 individual constellations for  $L = 41.5$  km (a) and  $L = 83$  km (b) spans. The violet (Polarization 1) and green (Polarization 2) curves are grouped per eigenvalue ( $\lambda_1 = i0.3$ ,  $\lambda_2 = i0.6$ ). (c) Comparison of the average BER versus transmission distance between links of the two different span lengths. The error bars represent the standard deviation over 5 processed blocks of  $10^5$  DP-NFDM symbols.

the optical front-end. The use of the PC was required to avoid the use of polarization tracking algorithms for the NFT signals, which were not available at the time of the experiment. In the future it could be possible to use modulation independent polarization tracking algorithms, as an example using independent components analysis [43]. The signal is then detected by using a standard coherent receiver (33 GHz analog bandwidth, 80 GSa/s), in a homodyne configuration where the transmitter laser is used as LO. The acquired digital signal consisting of 5 blocks of  $10^5$  DP-NFDM symbols is then fed to the receiver DSP chain described previously.

#### 4. EXPERIMENTAL RESULTS

The system was initially tested in a back-to-back (B2B) configuration, where the transmitter output has been directly connected to the receiver, in order to obtain the best performance achievable by the system in the sole presence of the intrinsic transceiver distortions (e.g. transmitter front-end distortions, detectors noise, etc.) and added additive white Gaussian noise (AWGN) as commonly done for linear coherent systems. The OSNR was swept by varying the noise power added to the signal at the receiver input. The adopted metric for measuring the performances allows a direct comparison with standard coherent transmission systems. The OSNR range considered is the region of interest where the system performance is around the HD-FEC threshold. The measured average BER is shown in Fig. 4. A visible effect is the fact that the BER is not the same for the four different constellations, but it is worse for the two constellations associated with the eigenvalue with a higher imaginary part. This effect can be related to the dependency of the noise variance of both the eigenvalues and the corresponding scattering coefficients on the imaginary part of the eigenvalues themselves [44–48]; an analysis of the noise distribution for the various eigenvalues and scattering coefficients is provided in the Supplementary Material.

In order to demonstrate fiber transmission with the proposed system, a transmission was performed over a link of  $N$  spans of SMF with span length  $L = 41.5$  and  $L = 83$  km. The performance in terms of BER as a function of the transmission distance is shown in Fig. 5 (a-b) for the four different constellations. The difference in performance in the two eigenvalues appears in this case too. This can also be seen from the constellation plots after 373.5 km in Fig. 6, where the two constellations associated with  $\lambda_2$  are sensibly more degraded than those related to  $\lambda_1$ , which

are still well defined. Similar performance can instead be seen in the two different polarizations of the same eigenvalue.

Finally in Fig. 5 (c) we compare the average BER for the two span lengths used in the test, in order to check the impact of the LPA approximation. Worse performances are expected when longer links are used being  $\gamma_{eff}$  given in Eq. (4) farther from the real  $\gamma$  of the fiber in this case. The BER curve for the 41.5 km span contains two outlier points at 124.5 km and 249 km that are slightly worse than the general trend of the curve. This is believed to be caused by instabilities in the setup when the related experimental traces were acquired, in particular an incorrect alignment of the polarization to the receiver due to a drift in the polarization state of the received signal. Besides these two points, the rest of the 41.5 km curve lies under the one for the 83 km spans, confirming that the use of longer spans adds a slight degradation in the performance of the system. The maximum reach of the system achieved with BER under the HD-FEC threshold is 373.5 km using 41.5 km spans and 249 km with spans of 83 km. It should be noted that in our experimental setup the PMD effect was not compensated for. However, for the transmission lengths and PMD values of the standard SMF employed, the accumulated differential group delay is negligible if compared with the pulse duration [4]. The impact of PMD is

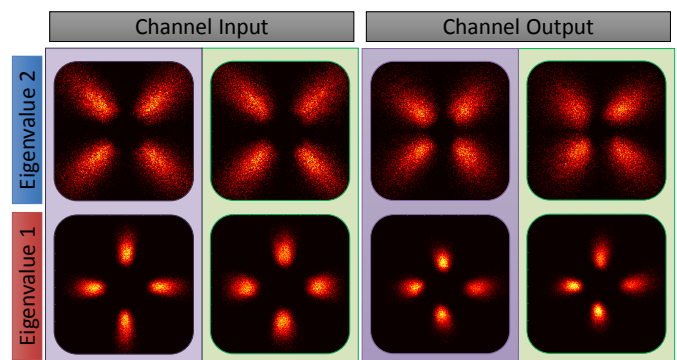


**Fig. 6.** The four experimental constellations of the scattering coefficients  $b_{1,2}(\lambda_i)$ ,  $i = 1, 2$  associated with the two eigenvalues ( $\lambda_1 = i0.3$ ,  $\lambda_2 = i0.6$ ) are shown at the transmitter side (left) and after 373.5 km transmission with 41.5 km spans (right). Polarization 1 and Polarization 2 on a violet and green background respectively.

therefore not expected to have had a major impact on the results shown. New approaches have been developed to compensate for PMD effects in linear transmission systems [49] and a recent work has shown in simulations that for a DP-NFDM system employing the continuous spectrum, PMD effects could be compensated in the nonlinear domain by using a linear equalizer [27]. Similar techniques may be applied to discrete DP-NFDM systems.

## 5. CONCLUSIONS

We have demonstrated experimentally, for the first time to the best of our knowledge, an eigenvalue-based optical communication system employing two orthogonal modes of polarization. We encoded 8 bits/DP-NFDM symbol and demonstrated transmission up to 373.5 km. Furthermore, we have shown that a powerful, but rather abstract mathematical technique, the Darboux transformation, can have indeed far-reaching impact in applied nonlinear optics namely in fiber-based telecommunication systems. Our results pave the way towards doubling the information rate of NFT-based fiber optics communication systems. Although more research work needs to be done in this direction, by demonstrating the possibility of using dual polarization NFT channels, we have indeed successfully met one of the key challenges that were explicitly highlighted in a recent review of this research field [8] as necessary steps in order to bring eigenvalue communication from a pioneering stage to be a working infrastructure for optical communications in the real-world. Furthermore, the demonstration of the polarization division multiplexing is a significant step forward towards a fair comparison of the NFT-based channels with the currently used linear ones where polarization division multiplexing is an established practice.

## FUNDING INFORMATION

This work was supported by the Marie Curie Actions through ICONE Project (no. 608099), the DNR Research Centre of Excellence, SPOC (no. DNR123) and the Villum foundation.

## ACKNOWLEDGMENTS

The authors thank S.K. Turitsyn, M. Kamalian, Y. Prylepskiy, R. T. Jones and J. Diniz for the stimulating discussions, constant encouragement and careful reading of the manuscript and the anonymous reviewers for their constructive criticism and relevant suggestions that improved the quality of the manuscript.

See Supplement 1 for supporting content.

## REFERENCES

1. E. Agrell, M. Karlsson, A. R. Chraplyvy, D. J. Richardson, P. M. Krummrich, P. Winzer, K. Roberts, J. K. Fischer, S. J. Savory, B. J. Eggleton, M. Secondini, F. R. Kschischang, A. Lord, J. Prat, I. Tomkos, J. E. Bowers, S. Srinivasan, M. Brandt-Pearce, and N. Gisin, "Roadmap of optical communications," *Journal of Optics* **18**, 063002 (2016).
2. P. P. Mitra and J. B. Stark, "Nonlinear limits to the information capacity of optical fiber communications," *Nature* **411**, 1027–1030 (2001).
3. R. J. Essiambre, P. J. Kramer, G. J. Foschini, and B. Goebel, "Capacity limits of optical fiber networks," *J. Lightwave Technol.* **28**, 662–701 (2010).
4. G. P. Agrawal, *Nonlinear Fiber Optics* (Academic Press, 2013), 5th ed.
5. A. D. Ellis, M. Tan, M. A. Iqbal, M. A. Z. Al-Khateeb, V. Gordienko, G. S. Mondaca, S. Fabbri, M. F. C. Stephens, M. E. McCarthy, A. Perentos, I. D. Phillips, D. Lavery, G. Liga, R. Maher, P. Harper, N. Doran, S. K. Turitsyn, S. Sygletos, and P. Bayvel, "4 Tb/s transmission reach enhancement using  $10 \times 400$  Gb/s super-channels and polarization insensitive dual band optical phase conjugation," *J. Lightwave Technol.* **34**, 1717–1723 (2016).
6. E. Ip and J. Kahn, "Compensation of dispersion and nonlinear impairments using digital backpropagation," *J. Lightwave Technol.* **26**, 3416–3425 (2008).
7. A. Hasegawa and T. Nyu, "Eigenvalue communication," *J. Lightwave Technol.* **11**, 395–399 (1993).
8. S. K. Turitsyn, J. E. Prilepsky, S. T. Le, S. Wahls, L. L. Frumin, M. Kamalian, and S. A. Derevyanko, "Nonlinear Fourier transform for optical data processing and transmission: advances and perspectives," *Optica* **4**, 207–322 (2017).
9. N. J. Ablowitz, D. J. Kaup, A. C. Newell, and H. Segur, "The inverse scattering transform-Fourier analysis for nonlinear problems," *Stud. Appl. Math.* **53**, 249–315 (1974).
10. V. E. Zakharov and A. B. Shabat, "Exact theory of 2-dimensional self-focusing and one-dimensional self-modulation of waves in nonlinear media," *Sov. Phys. J. Exp. Theor. Phys.* **34**, 62–69 (1972).
11. M. I. Yousefi and F. R. Kschischang, "Information transmission using the nonlinear Fourier transform, part I: Mathematical tools," *IEEE Transactions on Information Theory* **60**, 4312–4328 (2014).
12. H. Bülow, "Experimental demonstration of optical signal detection using nonlinear Fourier transform," *J. Lightwave Technol.* **33**, 1433–1439 (2015).
13. J. E. Prilepsky, S. A. Derevyanko, K. J. Blow, I. Gabitov, and S. K. Turitsyn, "Nonlinear inverse synthesis and eigenvalue division multiplexing in optical fiber channels," *Phys. Rev. Lett.* **113**, 013901 (2014).
14. S. T. Le, I. D. Phillips, Prilepsky, P. Harper, A. D. Ellis, and S. K. Turitsyn, "Demonstration of nonlinear inverse synthesis transmission over transoceanic distances," *J. Lightwave Technol.* **34**, 2459–2466 (2016).
15. V. Aref, H. Bülow, K. Schuh, and W. Idler, "Experimental demonstration of nonlinear frequency division multiplexed transmission," in "41st European Conference on Optical Communications (ECOC), paper Tu.1.1.2," (2015).
16. V. Aref, S. T. Le, and H. Bülow, "Demonstration of fully nonlinear spectrum modulated system in the highly nonlinear optical transmission regime," in "42st European Conference on Optical Communications (ECOC), paper Th.3.B.2," (2016).
17. P. K. Wai, C. R. Menyuk, and H. H. Chen, "Stability of solitons in randomly varying birefringent fibers," *Optics letters* **16**, 1231–3 (1991).
18. S. V. Manakov, "On the theory of two-dimensional stationary self-focusing of electromagnetic waves," *Soviet Physics JETP* **38**, 248–253 (1974).
19. J. Yang, "Multisoliton perturbation theory for the Manakov equations and its applications to nonlinear optics," *Physical Review E* **59**, 2393 (1999).
20. T. Lakoba and D. Kaup, "Perturbation theory for the manakov soliton and its applications to pulse propagation in randomly birefringent fibers," *Physical Review E* **56**, 6147 (1997).

21. C. Xie, M. Karlsson, P. A. Andrekson, H. Sunnerud, and J. Li, "Influences of polarization-mode dispersion on soliton transmission systems," *IEEE Journal of selected topics in quantum electronics* **8**, 575–590 (2002).
22. Y. Chen and H. Haus, "Manakov solitons and polarization mode dispersion," *Chaos: An Interdisciplinary Journal of Nonlinear Science* **10**, 529–538 (2000).
23. T. P. Horikis and J. N. Elgin, "Nonlinear optics in a birefringent optical fiber," *Physical Review E* **69**, 016603 (2004).
24. S. A. Derevyanko, J. E. Prilepsky, and D. A. Yakushev, "Statistics of a noise-driven Manakov soliton," *Journal of Physics A: Mathematical and General* **39**, 1297 (2006).
25. F. Baronio, A. Degasperis, M. Conforti, and S. Wabnitz, "Solutions of the vector nonlinear Schrödinger equations: evidence for deterministic rogue waves," *Physical review letters* **109**, 044102 (2012).
26. A. Maruta and Y. Matsuda, "Polarization division multiplexed optical eigenvalue modulation," in "International Conference on Photonics in Switching (PS)", Florence, Italy pp. 265–267 (2015).
27. J.-W. Goossens, M. I. Yousefi, Y. Jaouën, and H. Hafermann, "Polarization-division multiplexing based on the nonlinear Fourier transform," *Opt. Express* **25**, 26437–26452 (2017).
28. S. Gaiarin, A. M. Perego, E. Porto da Silva, F. Da Ros, and D. Zibar, "Experimental demonstration of dual polarization nonlinear frequency division multiplexed optical transmission system," in "43st European Conference on Optical Communications (ECOC), paper W.3.C.2," (2017).
29. C. R. Menyuk and B. S. Marks, "Interaction of polarization mode dispersion and nonlinearity in optical fiber transmission systems," *J. Lightwave Technol.* **24**, 2806 (2006).
30. M. J. Ablowitz, B. Prinari, and A. D. Trubatch, "Integrable nonlinear Schrödinger systems and their soliton dynamics," *Dynamics of PDE* **1**, 239–299 (2004).
31. R. G. Docksey and J. N. Elgin, "Closure of the Manakov system," *SIAM Journal on Mathematical Analysis* **32**, 54 (2000).
32. A. Hasegawa and Y. Kodama, "Guiding-center soliton in optical fibers," *Opt. Lett.* **15**, 1443–1445 (1990).
33. S. T. Le, J. E. Prilepsky, and S. K. Turitsyn, "Nonlinear inverse synthesis technique for optical links with lumped amplification," *Opt. Express* **23**, 8317–8328 (2015).
34. M. Kamalian, J. E. Prilepsky, S. T. Le, and S. K. Turitsyn, "On the design of NFT-based communication systems with lumped amplification," *J. Lightwave Technol.* **35**, 5464–5472 (2017).
35. T. Gui, T. H. Chan, C. Lu, A. P. T. Lau, and P. K. A. Wai, "Alternative decoding methods for optical communications based on nonlinear Fourier transform," *J. Lightwave Technol.* **35**, 1542–1550 (2017).
36. V. B. Matveev and M. A. Salle, *Darboux transformations and solitons* (Springer-Verlag, 1991).
37. M. I. Yousefi and F. R. Kschischang, "Information transmission using the nonlinear Fourier transform, part III: Spectrum modulation," *IEEE Transactions on Information Theory* **60**, 4346–4369 (2014).
38. O. C. Wright, "The Darboux transformation of some Manakov systems," *Applied Mathematics Letters* **16**, 647–652 (2003).
39. V. Aref, "Control and detection of discrete spectral amplitudes in nonlinear Fourier spectrum," arXiv:1605.06328 (2016).
40. T. Pfau, S. Hoffmann, and R. Noé, "Hardware-efficient coherent digital receiver concept with feedforward carrier recovery for MQAM constellations," *J. Lightwave Technol.* **27**, 989–999 (2009).
41. S. T. Le, V. Aref, and H. Buelow, "Nonlinear signal multiplexing for communication beyond the Kerr nonlinearity limit," *Nature Photonics* **2**, 1–8 (2017).
42. A. Hasegawa and Y. Kodama, *Solitons in optical communications*, 7 (Oxford University Press, USA, 1995).
43. N. Nabavi and T. J. Hall, "Demultiplexing by independent component analysis in coherent optical transmission: The polarization channel alignment problem," in "Photonics North," (2015).
44. Q. Zhang and T. H. Chan, "A Gaussian noise model of spectral amplitudes in soliton communication systems," in "Signal Processing Advances in Wireless Communications (SPAWC), 2015 IEEE 16th International Workshop on," (IEEE, 2015), pp. 455–459.
45. Q. Zhang and T. H. Chan, "A spectral domain noise model for optical fibre channels," in "IEEE International Symposium on Information Theory IEEE, Jun. 2015." pp. 1660–1664 (2015).
46. Q. Zhang and T. H. Chan, "Noise models in the nonlinear spectral domain for optical fibre communications," arXiv:1702.06226 (2017).
47. S. Hari and F. R. Kschischang, "Bi-directional algorithm for computing discrete spectral amplitudes in the NFT," *J. Lightwave Technol.* **34**, 3529–3537 (2016).
48. S. Hari, M. I. Yousefi, and F. R. Kschischang, "Multieigenvalue communication," *J. Lightwave Technol.* **34**, 3110–3117 (2016).
49. K. Kikuchi, "Analyses of wavelength-and polarization-division multiplexed transmission characteristics of optical quadrature-amplitude-modulation signals," *Opt. express* **19**, 17985–17995 (2011).